

Predicting Weak Lensing Statistics from Halo Mass Reconstructions

Spencer Everett

*Department of Physics, DePaul University,
SLAC National Laboratory**

(Dated: August 20, 2015)

As dark matter does not absorb or emit light, its distribution in the universe must be inferred through indirect effects such as the gravitational lensing of distant galaxies. While most sources are only weakly lensed, the systematic alignment of background galaxies around a foreground lens can constrain the mass of the lens which is largely in the form of dark matter. In this paper, I have implemented a framework to reconstruct all of the mass along lines of sight using a best-case dark matter halo model in which the halo mass is known. This framework is then used to make predictions of the weak lensing of 3,240 generated source galaxies through a 324 arcmin^2 field of the Millennium Simulation. The lensed source ellipticities are characterized by the ellipticity-ellipticity and galaxy-mass correlation functions and compared to the same statistic for the intrinsic and ray-traced ellipticities. In the ellipticity-ellipticity correlation function, I find that the framework systematically under predicts the shear power by an average factor of 2.2 and fails to capture correlation from dark matter structure at scales larger than 1 arcminute. The model predicted galaxy-mass correlation function is in agreement with the ray-traced statistic from scales 0.2 to 0.7 arcminutes, but systematically underpredicts shear power at scales larger than 0.7 arcminutes by an average factor of 1.2. Optimization of the framework code has reduced the mean CPU time per lensing prediction by 70% to $24 \pm 5 \text{ ms}$. Physical and computational shortcomings of the framework are discussed, as well as potential improvements for upcoming work.

I. INTRODUCTION

In a universe teeming with galaxies and light, it came as a shock when 20th century astronomers discovered that most of the mass in the universe is in fact dark; the ‘normal’ matter made of atoms that we interact with in everyday life, called baryonic matter, accounts for less than 20% of the mass in the observable universe. The remaining mass takes the form of an exotic dark matter that does not absorb or emit light, rendering it invisible to our telescopes. While this claim sounds bizarre, there has been an abundance of indirect evidence in recent decades for the existence of dark matter including the flattening of galaxy rotation curves [1], velocity dispersions of galaxies [2], and acoustic peaks in the cosmic microwave background [3].

One of the most successful probes of dark matter has been gravitational lensing. The path of light from distant ‘background’ galaxies is bent when traveling through regions of space containing large amounts of ‘foreground’ mass. Light from different origins in a source galaxy is subject to different bending which results in a distortion of the galaxy image. As the foreground mass is known to be largely dark matter, gravitational lensing supplies a direct constraint on the mass of dark matter in that region.

While the effects of gravitational lensing can be dramatic, the shape of most galaxies is only distorted by a few percent and must be detected statistically as the intrinsic shape is not known. If a model for the distribution of dark matter in a region of foreground mass can accu-

rately predict the statistical signal of this ‘weak’ lensing of background sources, then the model can be used on galaxies in existing sky survey data to extrapolate the amount of dark matter in the region and construct large-scale maps of the dark matter in the universe.

In this paper, I attempt to do the former by applying a simple dark matter halo model to reconstruct mass along lines of sight in the Millennium Simulation and predict the weakly lensed ellipticities of generated background sources. A brief introduction into the theory of galaxy ellipticities, the effects of strong and weak gravitational lensing, and dark matter halos is discussed in Section II. The implementation of a halo model on the Millennium Simulation is described in Section III, and the results of the model on 3,240 galaxies on a field size of 324 arcmin^2 , along with a comparison of the predicted lensed ellipticities to ray-traced ellipticities, is given in Section IV. Section V discusses limitations of the used framework as well as potential physical and computational improvements that can be made for upcoming work before concluding remarks in Section VI.

II. THEORETICAL BACKGROUND

Galaxies as Ellipses

Consider a galaxy image that can be well approximated as an ellipse at an angle ϕ above an arbitrary reference line. The galaxy’s complex ellipticity is defined to be

$$\varepsilon = \varepsilon_1 + i\varepsilon_2 = |\varepsilon| e^{2i\phi} \quad (1)$$

where the magnitude of the galaxy’s ellipticity $|\varepsilon|$ is de-

* spencerweverett@gmail.com

fined as

$$|\varepsilon| = \frac{1-r}{1+r} \quad (2)$$

and $r \leq 1$ is the ratio of the semi-minor and semi-major axes of the ellipse. This compact notation combines the eccentricity and orientation of the ellipse into a single object. A plot from Schneider et al. [4] showing the shape of elliptical galaxies for various values of ε_1 and ε_2 is shown in Figure 1a.

There are many complications to using this scheme in practice, most notably the multiplicative bias resulting from the smearing of galaxy images by the observational point spread function (PSF) [5]. While the effects of a PSF can be complex, in general it causes galaxy images to appear less elliptical than they truly are. To account for this in generated galaxy images, a multiplicative bias parameter M is often used to lessen the intrinsic ellipticity using

$$\varepsilon_{obs} = M \cdot \varepsilon_{int}$$

where ε_{int} is the generated intrinsic ellipticity of the image and ε_{obs} is the ellipticity that would be recorded by a detector.

Gravitational Lensing

A full mathematical treatment of the gravitational lensing of galaxies due to the gravitational fields of massive objects requires general relativity (see [7] for details). However, the important results can be summarized as follows. Foreground mass distorts the image of a background galaxy in two distinct ways: The image is magnified and sheared tangentially about the foreground mass, making it more elliptical. The magnification of the image is determined by the convergence κ , a scalar which measures the projected mass density along each line of sight. The shearing of the source is most often described by the complex shear γ defined to be

$$\gamma = \gamma_1 + i\gamma_2 = |\gamma| e^{2i\varphi} \quad (3)$$

where $|\gamma|$ is the magnitude of the shear and φ is the orientation of the shear. While the intrinsic ellipticities of source galaxies are randomly oriented near the foreground mass before lensing, they will be systematically more aligned with the shear field after lensing.

However, usually the quantity of interest in lensing calculations is the *reduced* shear, defined as

$$g = \frac{\gamma}{1-\kappa}. \quad (4)$$

Then using the thin lens approximation for the lensing of a background source of intrinsic ellipticity ε_i by foreground mass at a point with reduced shear g , the lensed

ellipticity ε is given by

$$\varepsilon = \begin{cases} \frac{\varepsilon_i + g}{1 + g^* \varepsilon_i} & : |g| \leq 1 \\ \frac{1 + g \varepsilon_i^*}{\varepsilon^* + g^*} & : |g| > 1 \end{cases} \quad (5)$$

where an asterisk denotes the complex conjugate [4]. The behavior of the distortion relies strongly on the magnitude of g ; the effect is called *strong* lensing if $|g| > 1$ and *weak* lensing if $|g| \leq 1$. The effects of strong lensing can be quite dramatic, distorting sources into large arcs, multiple images, or even an Einstein ring as shown in Figure 1b. While strong lenses are rare as the alignment of the source and foreground mass must be nearly perfect, *all* sources are weakly lensed. The effect is small, usually an ellipticity distortion of only a few percent, but can be detected locally by averaging the ellipticities of all sources in a small region. As the orientations of the sources should be random, it would be expected that

$$\langle \varepsilon \rangle = 0.$$

However, as sources in the same small region are sheared in (approximately) the same way, this implies that

$$\langle \varepsilon \rangle \approx g. \quad (6)$$

Finally as in the weak lensing regime $\kappa \ll 1$ and $|\gamma| \ll 1$, it follows that

$$\gamma \approx g \approx \langle \varepsilon \rangle \quad (7)$$

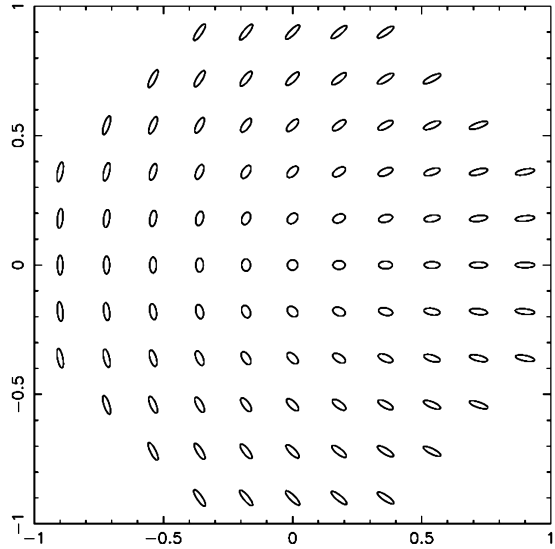
which provides a method of detecting the shear observationally.

Dark Matter Halos

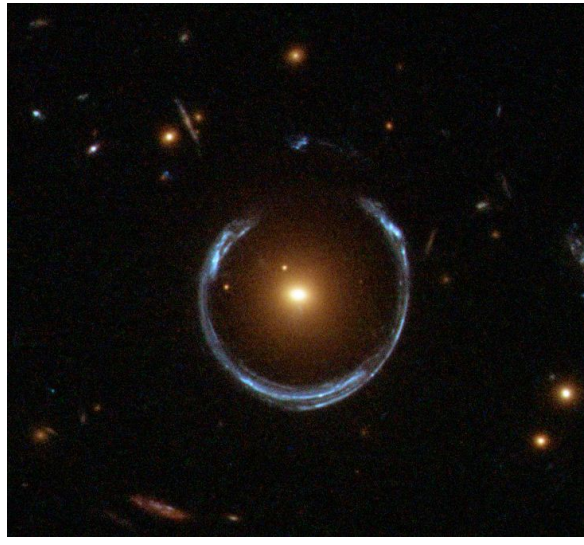
While the exact relation between the distribution of galaxies and dark matter is not known, simulations have shown that galaxies tend to form in over-dense regions of dark matter. This means that galaxies *should* trace out the larger underlying dark matter structures. The simplest way to model this relationship is by enveloping each galaxy in a spherically symmetric dark matter ‘halo’ of mass M_h sampled from the stellar-to-halo mass relation [8]. These halos extend far beyond the edge of the visible galaxy that they enclose. While the density profile of the halos may be complex, numerous simulations have shown that it can be well approximated by the Navarro-Frenk-White (NFW) profile which has the form

$$\rho_{NFW}(r) = \frac{\rho_0}{\frac{r}{R_s} \left(1 + \frac{r}{R_s}\right)^2} \quad (8)$$

where the constant ρ_0 and the scale radius R_s are parameters that vary from halo to halo [9]. This work uses a



(a) The shape of a galaxy image for various ellipticity components ε_1 and ε_2 on the x and y -axes respectively. Taken from [4].



(b) An image of the luminous red galaxy LRG 3-757 along with a strongly lensed background galaxy, called the ‘Cosmic Horseshoe’ [6].

FIG. 1

truncated NFW profile called the Baltz-Marshall-Oguri (BMO) profile given by

$$\rho_{BMO}(r) = \rho_{NFW} \cdot \left(\frac{r_t^2}{r^2 + r_t^2} \right)^2 \quad (9)$$

where r_t is a free parameter, as it has been shown to be a better fit to simulated data [10].

III. THE PANGLOSS FRAMEWORK

To constrain the mass of foreground dark matter using weak gravitational lensing, first a model of the relationship between foreground galaxies and the foreground dark matter must be established and robustly tested to see if, statistically, it makes the same lensing predictions of background sources as the true underlying dark matter structure. To do this, I built upon the publicly available **Pangloss** framework¹ used in Collett et al. [12] to reconstruct all the mass along the line of sight of each background galaxy using dark matter halos. The lensing contribution of each halo is calculated, and the total lensing of the background galaxy is the sum of each halo contribution. This process is detailed in the following sections.

Assumptions

While **Pangloss** may be used more generally, the present analysis makes some additional strong assumptions to simplify the problem for a first attempt at making weak lensing predictions.

1. The dark matter mass distribution can be approximated by spherically symmetric BMO halo profiles attached to each galaxy.
2. The stellar mass of the foreground galaxy is negligible for lensing calculations.
3. The mass of the dark matter halo of each foreground galaxy is known.
4. A spectroscopic redshift of each foreground galaxy is known.

Testing the first assumption is the main goal of this paper. The second assumption is reasonable as it is estimated that dark matter halos are on average 1-2 orders of magnitude more massive than the host galaxy [8]. Clearly the third assumption will never be true for any observational data. However, this allows for a best-case scenario estimate of how well the **Pangloss** framework *could* predict weak lensing effects given all possible information. This assumption can be relaxed by sampling a dark matter halo mass from an assumed stellar mass - halo mass relation. The fourth assumption is also unrealistic as most galaxies in sky surveys only have a less-reliable photometric redshift due to time constraints, but this again allows for a best-case estimate. This assumption could be relaxed by instead using photometric

¹ <https://github.com/drphilmarshall/Pangloss>

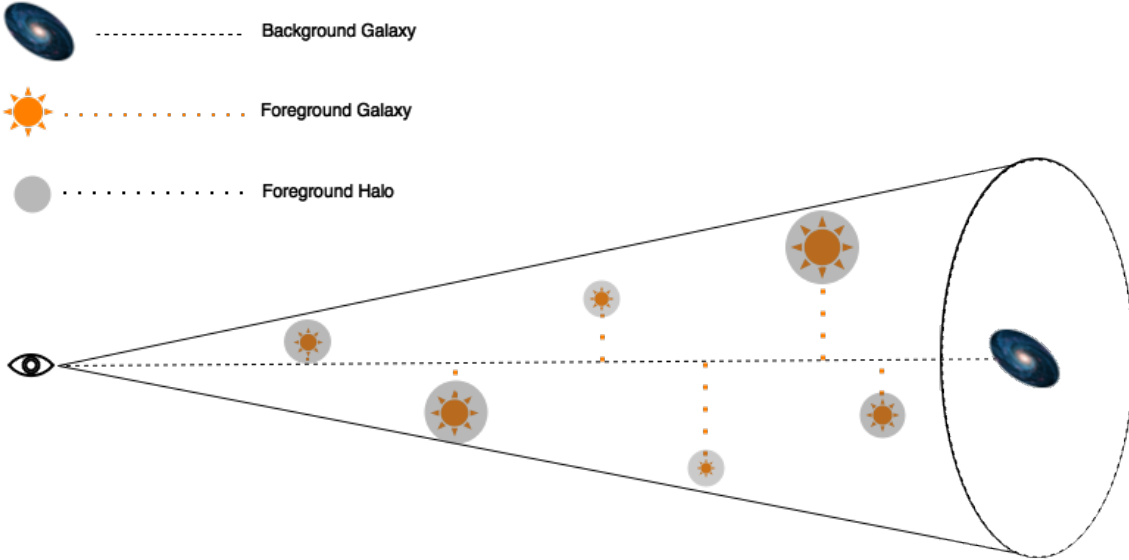


FIG. 2: A cartoon model of how the **Pangloss** framework uses a dark matter halo model to reconstruct the foreground mass along the line of sight of a background source galaxy. A ‘lightcone’ centered at a background source is constructed with radius R and populated with all foreground galaxies contained in this volume. Each foreground object has an attached dark matter halo and physical distance to the line of sight (dashed line). The shear and convergence along the line of sight contributed by each halo is calculated using [11], and the predicted ellipticity is determined using the sum of these contributions and Equation (5).

redshifts, adding random noise, and repeating the upcoming analysis on many realizations of the photometric redshifts.

The Millennium Simulation

Pangloss cannot be used to make dark matter mass maps using existing galaxy catalogs until it is tested on a simulated universe with known dark matter structure to determine how accurately and precisely it predicts the lensing of background sources. For this purpose, **Pangloss** was tested on galaxy catalogs from the Millennium Simulation, an N-body simulation consisting of over 10 billion dark matter ‘particles’ each representing a billion solar masses and populated with about 20 million galaxies [13]. The simulation uses cosmological parameters from WMAP 1st-year data analysis and contains baryonic and dark matter structure believed to be consistent with our own universe. From the work of Hilbert et al. [14], high resolution maps of the ray-traced shear and convergence are publicly available. From these maps, the actual lensing of background galaxies when traveling through the foreground mass of the Millennium Simulation can be calculated using Equation (5).

Generating Background Galaxies

With a catalog of foreground galaxies chosen, a set of 3,240 background galaxies over a field of 324 arcmin² was

generated, with density 10 per arcmin². The intrinsic orientation of each galaxy was sampled from a uniform distribution as, without lensing, there should be no preferred orientation due to the assumption of an isotropic universe. The magnitude of the galaxy ellipticities was sampled from a normal distribution with a standard deviation of 0.2, but any ellipticities with magnitude greater than one were re-sampled. Random ellipticity noise was sampled from a normal distribution with a standard deviation of 0.1 and added to the intrinsic ellipticities. Finally, each ellipticity was multiplied by $M = 0.9$ to account for a multiplicative bias of 10%.

Creating Lightcones

While ideally all foreground mass in a field would be considered when predicting the weak lensing of a background galaxy, it is computationally prohibitive to do so. Instead, all foreground halos contained within a ‘lightcone’ centered along the line of sight to the source and extending out to a chosen lightcone radius R were considered when calculating the lensing contributions for the background source. A cartoon model of this process is shown in Figure 2. Unless otherwise specified, experiments in this paper used a radius of 2 arcminutes.

To calculate the convergence and shear contribution of each halo, the physical distance from the halo to the line of sight was needed. To increase the speed of distance calculations, the foreground halo redshifts were first snapped to a grid of 100 equally-sized redshift bins

and then converted to physical distance.

Using the physical separation distance and halo mass, the shear and convergence contribution of a single foreground halo is calculated using methods described in Wright and Brainerd [11]. The total convergence and shear at the center of the lightcone is simply the sum of the convergence and shear contributions of each halo contained in the lightcone. The **Pangloss** predicted lensed source ellipticity is then calculated using Equation (5).

Checking the Halo Model

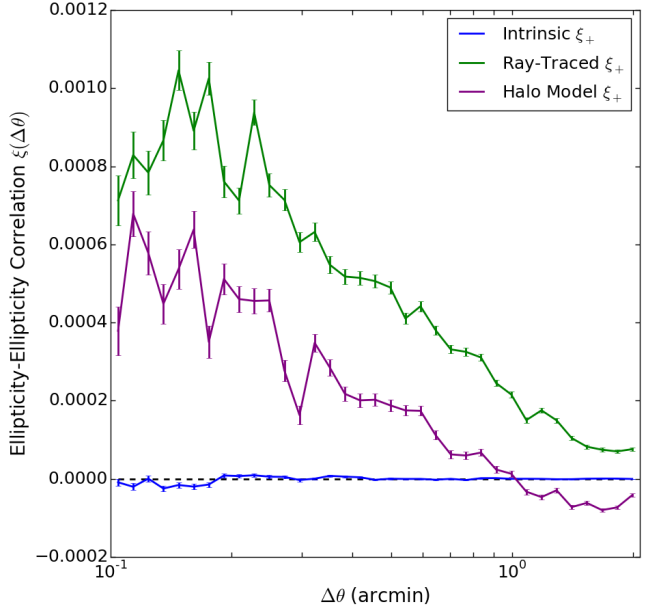
Instead of comparing the ray-traced and **Pangloss** predicted ellipticities for individual galaxies, the lensing is characterized globally with correlation functions. The ellipticity-ellipticity correlation function measures how correlated the ellipticities of pairs of galaxies are as a function of separation distance, while the galaxy-mass correlation function measures the correlation of lensed ellipticities around foreground halos as a function of separation distance. For readers that are unfamiliar with correlation functions in the context of cosmology or want a visual aid, see the appendix. Both correlation functions are used in this work to measure how well the **Pangloss** framework models weak lensing by dark matter structures using the publicly available **TreeCorr** module written by Mike Jarvis². Note that the ellipticity-ellipticity correlation function definition used in **TreeCorr** is slightly different than that used in most of the literature; for a derivation of the connection between Jarvis's definition and the more common Schneider definition [4], visit the **Pangloss** repository¹.

IV. RESULTS

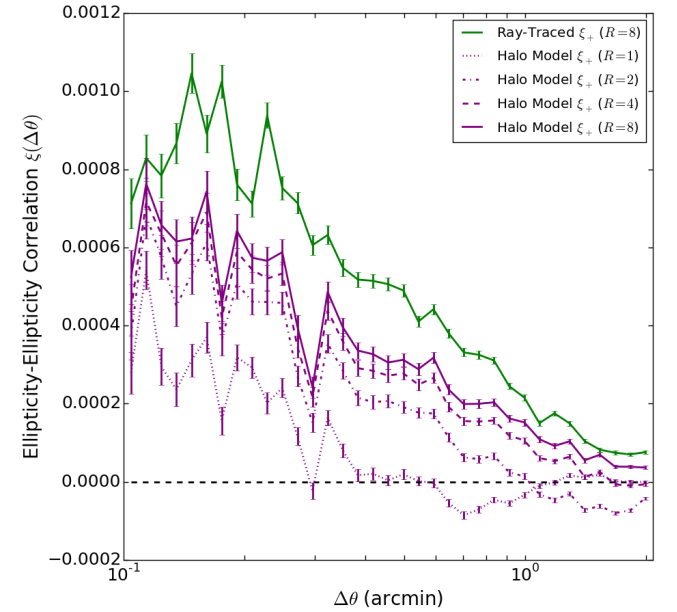
Using the presented methodology, 3,240 background galaxies in a 324 arcmin² subset of the (0,0,0,0) Millennium Simulation foreground catalog were generated and lensed by both the ray-traced shear and convergence maps as well as the **Pangloss** framework. With a lightcone radius of 2 arcminutes, the lightcones contained an average of 950 ± 70 foreground halos. Both sets of lensed ellipticities were characterized with correlation functions, as well as the intrinsic ellipticities of the sources before lensing.

Ellipticity-Ellipticity Correlation Function

The first test of the halo model was with the ellipticity-ellipticity correlation function with a lightcone radius of 2 arcminutes which is given in Figure 3a. The statistic



(a) The ellipticity-ellipticity correlation function for 3,240 sources at separation distances from 0.1 to 2 arcminutes and a lightcone radius of $R = 2$ arcminutes. While the correlation of the intrinsic ellipticities before lensing (blue) shows no correlation, the correlation of the ray-traced ellipticities (green) and halo model predicted ellipticities (purple) both show significant positive correlation on scales up to 1 arcminute. The halo model predicts a small negative correlation above this scale, while the ray-tracing shows positive correlation on all scales.



(b) The ellipticity-ellipticity correlation functions for a series of halo model frameworks with increasing lightcone radii from $R = 1$ to $R = 8$ arcminutes, all plotted in purple with various line styles. These are compared to the same ray-traced correlation from Figure 3a.

FIG. 3

² <https://github.com/rmjarvis/TreeCorr>

measured the average correlation between pairs of ellipticities at separation distances between 0.1 and 2 arcminutes. The correlation function of the intrinsic ellipticities plotted in blue shows no significant deviation from zero as expected, as before lensing the galaxies had random orientations. Both the ray-traced, plotted in green, and halo model, plotted in purple, ellipticities show positive correlation on small scales up to a separation of 1 arcminute. However, the ray-traced correlation is positive on all calculated scales while the halo model does not predict any significant correlation at separations above 1 arcminute. Additionally, while the shapes of the correlation functions for both sets of lensed ellipticities agree well until 1 arcminute, there is a clear systematic under-prediction of shear power by the halo model on all scales. On average, the shear power is underpredicted by 117%.

Using the same catalog of background sources, this statistic was recalculated for the halo model ellipticities for various lightcone radii ranging from $R = 1$ to $R = 8$ arcminutes. The result is shown in Figure 3b, where the series of model predicted correlation functions is compared to the ray-traced correlation function. As R increases, the mean number of foreground galaxies contained in each lightcone grows quadratically from 240 ± 25 galaxies when $R = 1$ arcminute to $15,000 \pm 300$ galaxies when $R = 8$ arcminutes. Increasing the number of foreground objects, and thus increasing the mass and structure considered for shear and convergence predictions, systematically increased the predicted shear power on all scales. While the series of predicted correlation functions appear to be converging towards the ray-traced correlation function, there is clearly diminishing shear power gains as R increases.

Galaxy-Mass Correlation Function

The catalog of lensed ellipticities was also analyzed using the galaxy-mass correlation function with separation distances from 0.1 to 2 arcminutes and a lightcone radius of 2 arcminutes. The result is shown in Figure 4. As with the ellipticity-ellipticity correlation function, there is no significant correlation for the intrinsic ellipticities at any scale as expected. The lensed ellipticities from the ray-tracing and halo model both show positive correlation on all calculated scales and are in agreement on separations from 0.2 to 0.7 arcminutes. However, the halo model is still systematically underpredicting the shear power on scales above 0.7 arcminutes, although now only by an average of 23%. A new feature is the large overprediction of shear power on separation scales smaller than 0.2 arcminutes. However, background sources this close to foreground halos are often in the strong lensing regime which is not currently accounted for by the `Pangloss` framework.

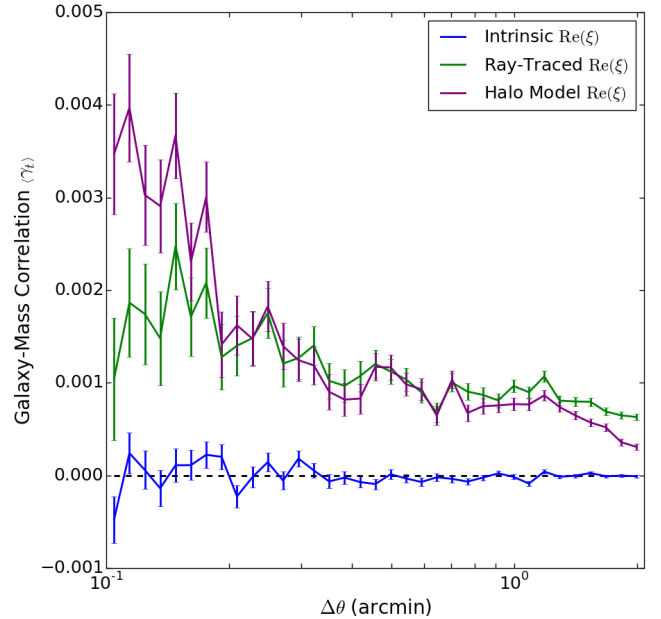


FIG. 4: The galaxy-mass correlation function of 3,240 sources at separation distances from 0.1 to 2 arcminutes and a lightcone radius of $R = 2$ arcminutes. There is no significant correlation of the intrinsic ellipticities (blue) as expected, and both the ray-traced correlation (green) and halo model correlation (purple) are positive on all scales. The green and purple curves are in agreement from 0.2 to 0.7 arcminutes, but have significant discrepancies on scales above and below this range.

Computational Performance

A secondary goal of this research was to investigate how quickly the prediction for the shear and convergence for a single background source could be made. The mean CPU time required for the prediction per lightcone was 80 ± 10 ms for the first run. However, many small improvements to the coding infrastructure of `Pangloss` were made to speed up the prediction. The average CPU time for a lensing prediction per lightcone for four separate runs after various (and cumulative) changes is plotted in Figure 5, with a final run time of 24 ± 5 ms. Run 1 corresponds to the original `Pangloss` framework code, run 2 only wrote the needed quantities for this analysis to the catalog `Astropy` tables, run 3 changed the redshift grid binning to be done once for all halos in the drilling rather than for every individual halo in lensing, and run 4 optimized various lensing calculations with matrices whenever possible. Cumulatively, these changes alone accounted for a 70% decrease in mean CPU time per lightcone and halved the initial variation.

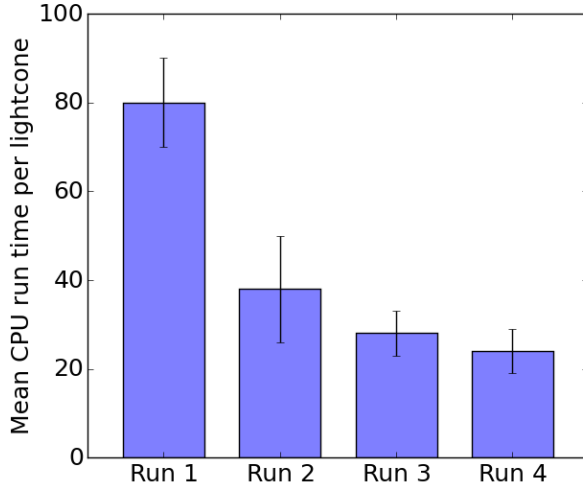


FIG. 5: The mean CPU runtime for various runs with different (and cumulative) code optimizations described in the text. The cumulative changes account for a 70% decrease in the mean CPU time and a halving of the variation. Currently, the prediction can be made for a single lightcone in 24 ± 5 ms.

V. DISCUSSION

Issues with the Pangloss Framework

Both the ellipticity-ellipticity and galaxy-mass correlation functions show clear issues with using the halo model to predict the lensing of background sources with **Pangloss**, even in the best-case scenario of perfect knowledge of the halo masses and their spectroscopic redshifts. The systematic underprediction of shear power present in both correlation functions is likely due to missing features in the model such as clusters, filaments, and voids.

While individual galaxies currently receive halos, a cluster of galaxies will sit in a larger halo whose presence is not being considered as its position, mass, and extent are difficult to determine. The absence of this mass undoubtedly effects shear predictions and ellipticity correlations on large scales. While some of the filament structure is captured in the framework, as the higher density of galaxies in filaments will lead to a higher density of halos, any additional dark matter structure between halos and clusters is not being accounted for. While difficult to do in practice, one can imagine connecting clusters of galaxies with dark matter ‘cylinders’ to account for the extra filament mass. Voids are also not currently considered, as the framework assumes the field has constant mass density equal to that of the average mass density of the universe and then adds halo masses on top of this density. This would make the average matter density across the field *larger* than the mean density of the universe, and

could be counteracted by subtracting mass from regions in between foreground halos. Stellar masses could also be incorporated into the **Pangloss** prediction, but any effect would likely be dominated by the missing features described above.

The progression of model predicted ellipticity-ellipticity correlation functions at larger radii converging to the ray-traced correlation in Figure 3b supports the analysis given above, as the prediction was progressively better with larger number of foreground halos and thus more mass and structure. However, the number of foreground objects scales quadratically with the lightcone radius making it prohibitively expensive above $R = 8$ arcminutes. With a radius this large, most foreground objects will be too far away from the line of sight and have insufficient mass to make a significant contribution to the lensing of the background source. This suggests the creation of a metric to predict the ‘relevance’ of each halo to the lensing contribution. In this way, the framework could be restructured to only use the most important halos in the computationally expensive lensing prediction, while simultaneously allowing for larger lightcones with more relevant halos. This could aid in the aforementioned shear power prediction issues.

Scaling Up Pangloss

While the current **Pangloss** framework can handle the lensing predictions of 3,240 sources in a 324 arcmin^2 field comfortably on a single processor, the goal is to scale up the framework to make predictions for background sources of the same number density in a 100 deg^2 field; this will require 3.6 million lightcones, each containing up to 1,000 foreground halos. Luckily, the prediction is trivially parallelizable as the shear and convergence calculation of each lightcone is independent of all other lightcones. This makes GPUs an attractive candidate for future work, as it would only take 360 GPUs with 10,000 threads each to carry out the prediction. Additionally, the 50 MB of RAM per lightcone is sufficiently small to fit 10,000 lightcones on a GPU.

VI. CONCLUSION

In this paper, a simple halo model was used to reconstruct all the mass along lines of sight in the Millennium Simulation to make predictions of how foreground mass weakly lensed the ellipticities of 3,240 generated background sources across a field of 324 arcmin^2 . The lensed ellipticities were characterized globally using the ellipticity-ellipticity and galaxy-mass correlation functions and then compared with the same statistics from ray-traced data. There was a systematic-underprediction of shear power on all scales in the ellipticity-ellipticity correlation function as well as an absence of any predicted correlation on scales larger than 1 arcminute, sug-

gesting missing features in the Pangloss framework. The galaxy-mass correlation function predicted by the halo model was in agreement with the ray-traced correlation function on scales from 0.2 to 0.7 arcminutes, but significantly overpredicted the shear power on smaller scales due to strong lensing effects. Now that a proof of concept has been demonstrated, there is work being done to scale up the Pangloss framework to make lensing predictions over 100 deg² using far more computational resources. While the results are encouraging for such a simple model, many strong and unrealistic assumptions were made in the methodology that limit its use in observational surveys. In the future, a similar analysis should be made after relaxing some of the assumptions to see how different the predictions by the halo model are from this best-case scenario.

VII. ACKNOWLEDGEMENTS

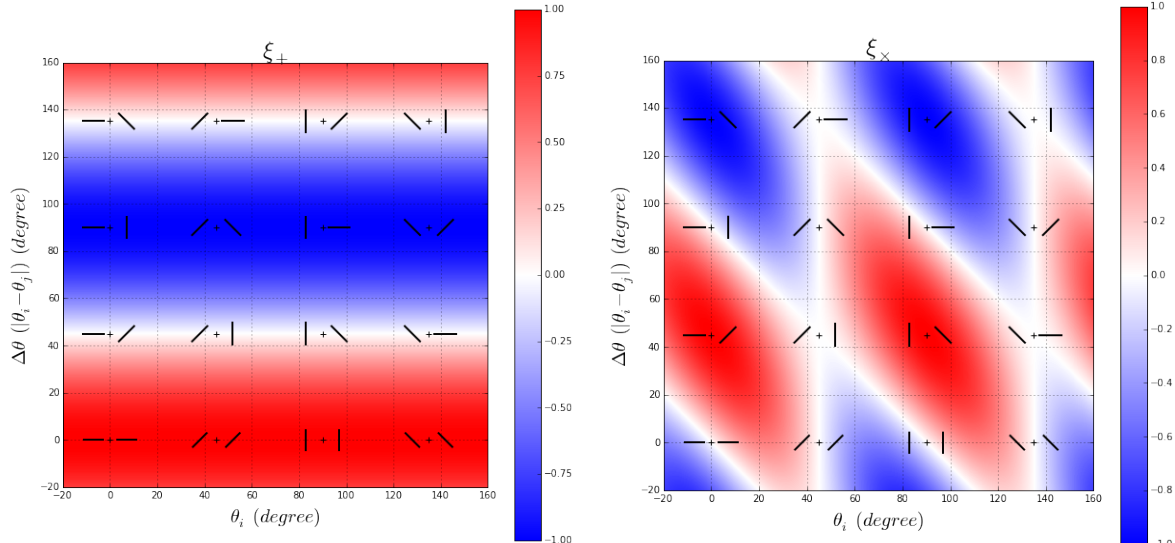
I would like to thank the Department of Energy for funding this research and giving me this wonderful opportunity, as well as SLAC National Laboratory for hosting me. This work was greatly aided by numerous conversations with Risa Wechsler from Stanford University and Matt Becker from the Kavli Institute for Particle Astrophysics and Cosmology (KIPAC). Finally, I am incredibly grateful to Phil Marshall for his unending support, patience, and guidance throughout this research. This work was supported in part by the U.S. Department of Energy, Office of Science, Office of Workforce Development for Teachers and Scientists (WDTS) under the Science Undergraduate Laboratory Internships Program (SULI).

VIII. APPENDIX

Visualizing Correlation Functions

At first encounter, the use of correlation functions to analyze data can be difficult to comprehend, let alone visualize. While by no means a thorough or mathematical analysis (see [15] for a more formal introduction), I have created some explanatory plots to aid in visualizing how weakly lensed ellipticities can be measured with correlation functions and place the main results of this paper in more context.

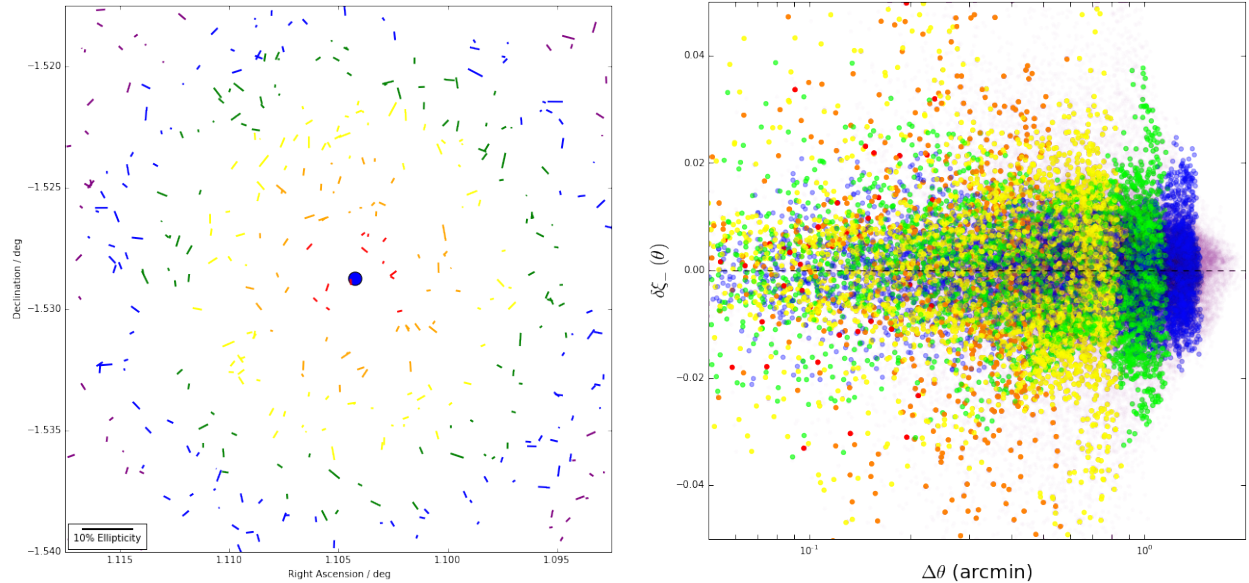
The main statistic used in this work is the ellipticity-ellipticity ($\varepsilon - \varepsilon$) correlation function, which has two tangential components ξ_{\pm} and a cross component ξ_{\times} . The components most interesting for gravitational lensing are the positive tangential component ξ_+ , expected to be positive for lensed galaxies, and the cross component ξ_{\times} , which is expected to be zero. To get an intuition for what these quantities measure, first consider the correlation values for individual pairs of galaxies as shown in Figure 6. In each plot, the value of the correlation between two galaxies as a function of



(a) The positive tangential component of the $\varepsilon - \varepsilon$ correlation as a function of galaxy orientation plotted as a colormap. The correlation component is positive for parallel galaxies, negative for perpendicular galaxies, and zero for galaxies offset by 45°.

(b) The cross component of the $\varepsilon - \varepsilon$ correlation as a function of galaxy orientation plotted as a colormap. While the pattern is more complicated than that of the tangential component, note that the correlation is zero for all preferred orientations after lensing.

FIG. 6: Correlation pair colormaps for ξ_+ and ξ_{\times} .



(a) A set of background sources around a foreground lens (blue dot). The size and orientation of each stick represents the intrinsic source ellipticity and is colored by the distance away from the lens.

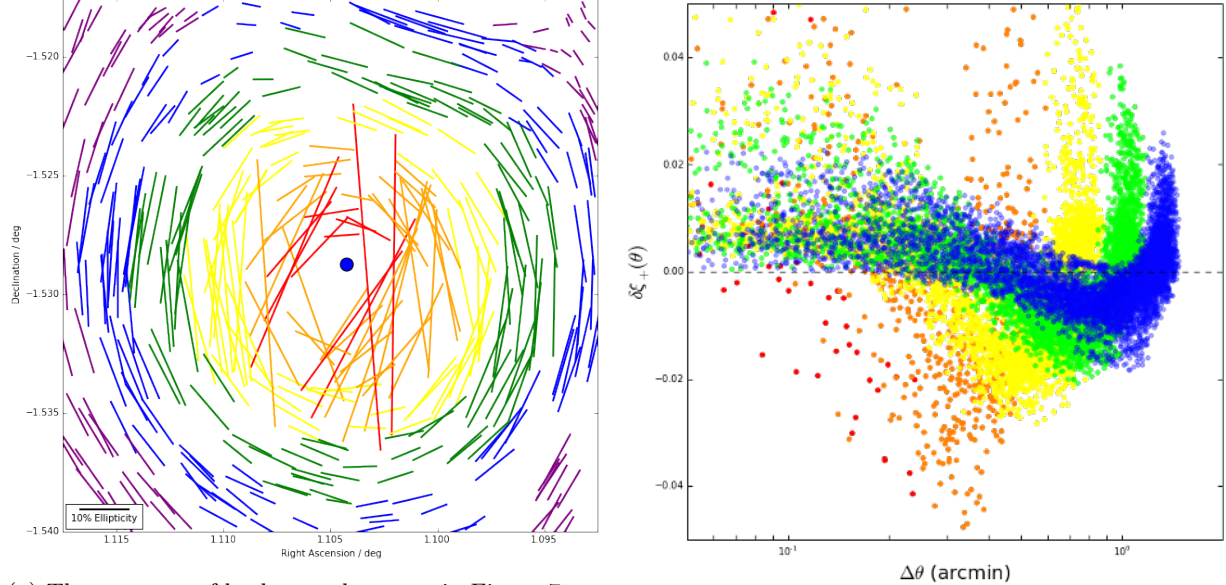
(b) The distribution of correlation pairs from the source ellipticities in Figure 7a. If the pair of galaxies are in the same color bin, then the correlation scatter point is colored in the same scheme.

FIG. 7: Correlation visualization for un-lensed galaxies.

their relative orientation is plotted as a colormap with a few sampled galaxy orientations superimposed. For ξ_+ the correlation is positive for parallel galaxies, negative for perpendicular galaxies, and zero for galaxies offset by 45° . In contrast, ξ_\times is zero for all parallel and perpendicular orientations while nonzero for most 45° offsets. As gravitational lensing shears source images tangentially around a foreground mass, the tangential component is a measure of how similarly two galaxies are lensed, while the cross component is an estimate of the bias (as it should be zero).

Now consider a region of space around a foreground lens populated with many background sources *before lensing*, as in Figure 7a. In this plot, source ellipticities are plotted as sticks and colored by their distance from the lens. Calculating the ξ_+ component correlation pairs for all galaxies in the same color bin and making a scatter plot as a function of the separation distance between the source pairs, we find the distribution in Figure 7b. The ξ_+ component of the $\varepsilon - \varepsilon$ correlation function is simply the average of this scatter plot binned in separation distances along the x -axis. As the scatter is randomly distributed around zero, the $\varepsilon - \varepsilon$ correlation function for un-lensed sources should be zero on all scales.

The same plots for the source galaxies *after lensing* are shown in Figure 8. The source ellipticities have clearly aligned tangentially around the foreground lens in Figure 8a, and distinct patterns have appeared in the correlation pair distribution for each color bin in Figure 8b. First consider a single color bin, such as the blue. Galaxies next to one another are lensed in approximately the same way and thus nearly parallel, leading to a positive correlation at small separation distances in Figure 8b. Moving a quarter of the way around the blue circle of galaxies, the lensed ellipticities become perpendicular and have negative correlation. This can be seen as the dip in correlation at ‘middle’ separation distances in 8b. Finally for galaxies on opposite sides of the lens, their relative orientation is again parallel and the correlation has returned to positive values. This spike in correlation is clearly visible in the distribution and is shifted to the right for colors further from the lens as the radius of the color bin increases. Averaging all scatter points in discrete separation distance bins, the $\varepsilon - \varepsilon$ correlation function will no longer be zero and a detectable signal will remain.



(a) The same set of background sources in Figure 7a after (magnified for effect) lensing by the foreground mass. Regardless of initial orientation, the source galaxies have all at least partially aligned tangentially around the center lensing mass.

(b) The distribution of correlation pairs from the source ellipticities in Figure 8a. If the pair of galaxies are in the same color bin, then the correlation scatter point is colored in the same scheme.

FIG. 8: Correlation visualization for lensed galaxies.

IX. REFERENCES

- [1] V. C. Rubin, W. K. J. Ford, and N. . Thonnard. Rotational properties of 21 SC galaxies with a large range of luminosities and radii, from NGC 4605 /R = 4kpc/ to UGC 2885 /R = 122 kpc/. *Astrophys. J.*, 238:471–487, June 1980.
- [2] F. Zwicky. On the Masses of Nebulae and of Clusters of Nebulae. *Astrophys. J.*, 86:217, October 1937.
- [3] Planck Collaboration, R. Adam, P. A. R. Ade, N. Aghanim, Y. Akrami, M. I. R. Alves, M. Arnaud, F. Arroja, J. Aumont, C. Baccigalupi, and et al. Planck 2015 results. I. Overview of products and scientific results. *ArXiv e-prints*, February 2015.
- [4] P. Schneider. Weak Gravitational Lensing. *ArXiv Astrophysics e-prints*, September 2005.
- [5] E. S. Cypriano, A. Amara, L. M. Voigt, S. L. Bridle, F. B. Abdalla, A. Réfrégier, M. Seiffert, and J. Rhodes. Cosmic shear requirements on the wavelength dependence of telescope point spread functions. *MNRAS*, 405:494–502, June 2010.
- [6] V. Belokurov, N. W. Evans, A. Moiseev, L. J. King, P. C. Hewett, M. Pettini, L. Wyrzykowski, R. G. McMahon, M. C. Smith, G. Gilmore, S. F. Sanchez, A. Udalski, S. Koposov, D. B. Zucker, and C. J. Walcher. The Cosmic Horseshoe: Discovery of an Einstein Ring around a Giant Luminous Red Galaxy. *ApJ*, 671:L9–L12, December 2007.
- [7] S. Dodelson. *Modern Cosmology*. Academic Press. Academic Press, 2003.
- [8] A. Kravtsov, A. Vikhlinin, and A. Meshcheryakov. Stellar mass – halo mass relation and star formation efficiency in high-mass halos. *ArXiv e-prints*, January 2014.
- [9] D. Coe. Dark Matter Halo Mass Profiles. *ArXiv e-prints*, May 2010.
- [10] L. J. Bernaldo e Silva, M. Lima, and L. Sodré. Testing phenomenological and theoretical models of dark matter density profiles with galaxy clusters. *MNRAS*, 436:2616–2624, December 2013.
- [11] C. Oaxaca Wright and T. G. Brainerd. Gravitational Lensing by NFW Halos. *ArXiv Astrophysics e-prints*, August 1999.
- [12] T. E. Collett, P. J. Marshall, M. W. Auger, S. Hilbert, S. H. Suyu, Z. Greene, T. Treu, C. D. Fassnacht, L. V. E. Koopmans, M. Bradač, and R. D. Blandford. Reconstructing the lensing mass in the Universe from photometric catalogue data. *MNRAS*, 432:679–692, June 2013.
- [13] V. Springel, S. D. M. White, A. Jenkins, C. S. Frenk, N. Yoshida, L. Gao, J. Navarro, R. Thacker, D. Croton, J. Helly, J. A. Peacock, S. Cole, P. Thomas, H. Couchman, A. Evrard, J. Colberg, and F. Pearce. Simulations of the formation, evolution and clustering of galaxies and quasars. *Nature (London)*, 435:629–636, June 2005.
- [14] S. Hilbert, J. Hartlap, S. D. M. White, and P. Schneider. Ray-tracing through the Millennium Simulation: Born corrections and lens-lens coupling in cosmic shear and galaxy-galaxy lensing. *A&A*, 499:31–43, May 2009.
- [15] J. Miralda-Escude. The correlation function of galaxy ellipticities produced by gravitational lensing. *Astrophys. J.*, 380:1–8, October 1991.